
JR-GAN: Jacobian Regularization for Generative Adversarial Networks

Weili Nie
Rice University
wn8@rice.edu

Ankit B. Patel
Rice University, Baylor College of Medicine
abp4@rice.edu

Abstract

Generative adversarial networks (GANs) are notoriously difficult to train and the reasons for their (non-)convergence behaviors are still not completely understood. Using a simple GAN example, we mathematically analyze the local convergence behavior of its training dynamics in a non-asymptotic way. We find that in order to ensure a good convergence rate two factors of the Jacobian should be *simultaneously* avoided, which are (1) *Phase Factor*: the Jacobian has complex eigenvalues with a large imaginary-to-real ratio, (2) *Conditioning Factor*: the Jacobian is ill-conditioned. Previous methods of regularizing the Jacobian can only alleviate one of these two factors, while making the other more severe. From our theoretical analysis, we propose the Jacobian Regularized GANs (JR-GANs), which insure the two factors are alleviated by construction. With extensive experiments on several popular datasets, we show that the JR-GAN training is highly stable and achieves near state-of-the-art results both qualitatively and quantitatively.

1 Introduction

Generative adversarial networks (GANs) [1] have achieved great success at generating realistic samples, with extensive applications [2–4]. The goal of GANs is to generate samples that are indistinguishable from the real data and hence has essentially learned the underlying data distribution. However, they are difficult to train such that many heuristic tricks have been applied [5, 6]. As a result, a lot of theoretical work has focused on stabilizing the GAN training by replacing Jensen-Shannon (JS) divergence implicit in the vanilla GAN [1] with alternative divergences (or distances), such as f -divergence (i.e. f -GAN) [7] and Wasserstein distance (i.e. WGAN) [8]. Much of the related work has introduced various regularizers for better approximating these divergences [9–11].

But the training dynamics of GANs are still not completely understood. Typically, the training of GANs is achieved by solving the zero-sum game via simultaneous gradient descent (SimGD) or alternative gradient descent [1, 7, 8]. The original work [1] showed that the SimGD converges to the equilibrium if the updates are made in the function space. In practice, with the generator and discriminator being parametrized by two separate neural networks, the updates in the parameter space are no longer guaranteed to converge due to its highly non-convex properties [12].

Recently, [13] showed that under suitable assumptions, the GAN dynamics are locally convergent. Furthermore, [14] pointed out that if the assumptions in [13] are not satisfied, in particular when distributions are not absolutely continuous, the GAN dynamics are not always convergent, unless some regularization techniques are applied, such as zero-centered gradient penalties [10] and consensus optimization (ConOpt) [15]. However, these theoretical results are established in an asymptotic limit of vanishing step size where SimGD approximates a continuous-time dynamic system. In practice, we are more concerned about the characterization of the non-asymptotic convergence rate and the choice of the finite step size or learning rate. This is because that even though the continuous-time dynamic system is convergent, its discrete-time counterpart might still suffer from poor convergence.

For instance, [15] reported that training GANs via SimGD suffers due to the existence of complex eigenvalues in the Jacobian of the dynamic system.

In this work, we focus on the non-asymptotic analysis of local convergence in the GAN dynamics. By considering a simple GAN example, we evaluate the eigenvalues of its Jacobian near the equilibrium and provide the convergence rate. We find out that the number of iterations needed to achieve an ϵ -error solution might be unexpectedly large due to both the *Phase Factor* and *Conditioning Factor* of the Jacobian. We later show that previous methods of regularizing the Jacobian directly can only alleviate one of these two factors but at the same time make the impact of the other one more severe. Based on our analysis, we propose a new Jacobian regularization for GANs, called JR-GAN, and theoretically show that JR-GAN could help alleviate these two factors simultaneously in the above simple GAN example. Experimentally, JR-GAN is more robust to different choices of GAN architectures compared with previous training stabilization techniques, and could also achieve near start-of-the-art results for the unsupervised image generation on several popular datasets.

2 Background

2.1 GAN as a minimax game

Despite many variants, the GAN is best described as a minimax game in which the two players, usually named the generator and discriminator, are trying to maximize and minimize the same objective function, respectively. The GAN game is generally formulated as follows:

$$\begin{aligned} & \min_{\phi} \max_{\theta} f(\phi, \theta) \\ & f(\phi, \theta) \triangleq \mathbb{E}_{x \sim P_r}[g_1(D_\theta(x))] + \mathbb{E}_{z \sim P_0}[g_2(D_\theta(G_\phi(z)))] \end{aligned} \quad (1)$$

where $\phi \in \mathbb{R}^n$ and $\theta \in \mathbb{R}^n$ denote the parameters of the generator $G_\phi : \mathcal{Z} \rightarrow \mathcal{X}$ and discriminator $D_\theta : \mathcal{X} \rightarrow \mathbb{R}$, respectively, P_r and P_0 represent the true data distribution with support \mathcal{X} and the random noise distribution with support \mathcal{Z} . Besides, two functions $g_1, g_2 : \mathbb{R} \rightarrow \mathbb{R}$, determined by the implicit divergence or distance that the generator is supposed to minimize, are both concave functions according to f -GAN and WGAN. For example, we can choose to implicitly minimize JS divergence in the vanilla GAN with $g_1(t) = g_2(-t) = -\log(1 + e^{-t})$, Wasserstein distance in the WGAN with $g_1(t) = g_2(-t) = t$ and reverse Kullback–Leibler (KL) divergence with $g_1(t) = -e^{-t}, g_2(t) = 1 - t$.

For training the minimax GAN game (1), SimGD is the most commonly used algorithm, in which the parameter updates are

$$\begin{aligned} \phi^{(k+1)} &= \phi^{(k)} - \eta \nabla_{\phi} f(\phi^{(k)}, \theta^{(k)}) \\ \theta^{(k+1)} &= \theta^{(k)} + \eta \nabla_{\theta} f(\phi^{(k)}, \theta^{(k)}) \end{aligned} \quad (2)$$

where $\eta > 0$ is the step size, $\phi^{(k)}$ and $\theta^{(k)}$ denote the corresponding parameters in the k -th iteration. Due to the highly non-convex properties of the GAN objective [12], it is difficult to analyze its global convergence in general. To gain key insights into the training instabilities in GANs, we focus on the local convergence of points near the equilibrium [13–16].

2.2 Asymptotic vs. non-asymptotic convergence analysis

The asymptotic convergence analysis is defined as applying the “ordinary differential equation (ODE) method” to analyze the convergence properties of dynamic systems. For example, consider a discrete-time system characterized by the gradient descent $v^{(t+1)} = v^{(t)} + \eta h(v^{(t)})$ for the gradient $h(\cdot) : \mathbb{R}^n \rightarrow \mathbb{R}^n$ and step size $\eta > 0$, the asymptotic convergence analysis assumes the step size η is infinitely small such that the discrete-time system can be approximated by an ODE $\dot{v}(t) = h(v(t))$. According to the Linearization Theorem [17], if the Jacobian of the dynamic system $A \triangleq \frac{\partial h(v)}{\partial v}$ evaluated at a stationary point v^* is Hurwitz, namely, $\text{Re}\{\lambda_i(A)\} < 0, \forall i = 1, \dots, n$, the equivalent ODE will converge to v^* for all points in its neighborhood.

In the non-asymptotic convergence analysis, however, we consider the discrete system directly to obtain the number of iterations needed to achieve an ϵ -error solution with a finite step size. Particularly, given the Jacobian A , to ensure the non-asymptotic convergence, we first provide an appropriate range of step size η by solving the inequalities $|1 + \lambda_i(A)| < 1, \forall i = 1, \dots, n$. Based on the constraint of

the step size, we get the minimum value of $|1 + \lambda_i(A)|$, and thus are able to evaluate the minimum number of iterations for an ϵ -error solution, which characterizes the convergence rate. As we can see, the non-asymptotic analysis could more precisely reveal the convergence performance of the dynamic system than the asymptotic one.

3 A simple GAN example

We consider a simple GAN example, in which the true data distribution is an isotropic Gaussian with a nonzero mean, i.e. $x \sim \mathcal{N}(v, \sigma^2 I)$ where $x \in \mathbb{R}^n$ and noise distribution is also a Gaussian with the same shape but a zero mean, i.e. $z \sim \mathcal{N}(0, \sigma^2 I)$ where $z \in \mathbb{R}^n$. Unless otherwise stated, we assume $n \geq 2$, $\|v\|^2 > 2$ and $0 < \sigma^2 < 2$. In addition, we assume the generator and discriminator are both linear, i.e. $D_\theta(x) = \theta^T x$ and $G_\phi(z) = \phi + z$, which is obviously expressive enough to learn the true data distribution. Then the GAN game objective function in (1) can be rewritten as

$$f(\phi, \theta) = \mathbb{E}_{x \sim \mathcal{N}(v, \sigma^2 I)}[g_1(\theta^T x)] + \mathbb{E}_{z \sim \mathcal{N}(0, \sigma^2 I)}[g_2(\theta^T(\phi + z))] \quad (3)$$

It is easy to verify that the equilibrium exists, which is $(\phi^*, \theta^*) = (v, 0)$. First, by considering a small open neighborhood of (ϕ^*, θ^*) of radius δ , denoted by $B_\delta(\phi^*, \theta^*)$, we introduce the local properties in this simple GAN example as follows.

Lemma 1. *The first-order derivative of $f(\phi, \theta)$ with respect to $(\phi, \theta) \in B_\delta(\phi^*, \theta^*)$ is given by*

$$\nabla f(\phi, \theta) \triangleq \begin{bmatrix} \nabla_\phi f(\phi, \theta) \\ \nabla_\theta f(\phi, \theta) \end{bmatrix} \approx \begin{bmatrix} g_2'(0)\theta \\ (g_1''(0) + g_2''(0))(\sigma^2 I + vv^T)\theta + g_1'(0)v + g_2'(0)\phi \end{bmatrix} \quad (4)$$

and its second-order derivative for $(\phi, \theta) \in B_\delta(\phi^*, \theta^*)$ is given by

$$\nabla^2 f(\phi, \theta) \triangleq \begin{bmatrix} \nabla_{\phi\phi}^2 f(\phi, \theta) & \nabla_{\phi\theta}^2 f(\phi, \theta) \\ \nabla_{\theta\phi}^2 f(\phi, \theta) & \nabla_{\theta\theta}^2 f(\phi, \theta) \end{bmatrix} \approx \begin{bmatrix} g_2''(0)\theta\theta^T & g_2'(0)I \\ g_2'(0)I & (g_1''(0) + g_2''(0))(\sigma^2 I + vv^T) \end{bmatrix} \quad (5)$$

Proof: See Appendix A.1. \square

Due to the concavity of $g_1(x)$ and $g_2(x)$, we know $g_1''(0) \leq 0$ and $g_2''(0) \leq 0$. From (5) we will always have $\nabla_{\phi\phi}^2 f(\phi, \theta) \preceq 0$ and $\nabla_{\theta\theta}^2 f(\phi, \theta) \preceq 0$ for all points in the local region $B_\delta(\phi^*, \theta^*)$. Take the vanilla GAN objective as an example, we can easily get $g_1''(0) = g_2''(0) = -\frac{1}{4}$, so its objective is *concave-concave* in ϕ and θ , instead of being convex-concave as assumed in previous works [7, 18]. This makes the non-asymptotic convergence analysis not simplistic as the problem looks like.

Without loss of generality, we mainly consider the vanilla GAN objective, i.e. $g_1(t) = g_2(-t) = -\log(1 + e^{-t})$, in the rest of the paper. For simplicity, we let $w \triangleq \begin{bmatrix} \phi - v \\ \theta \end{bmatrix}$ so the equilibrium becomes $w^* = 0$ and the SimGD updates in (2) can be rewritten as

$$w^{(k+1)} = w^{(k)} + \eta \tilde{\nabla} f(w^{(k)}) \quad (6)$$

where $\tilde{\nabla} f(w^{(k)}) \triangleq \begin{bmatrix} -\nabla_\phi f(w^{(k)}) \\ \nabla_\theta f(w^{(k)}) \end{bmatrix}$, and the Jacobian is given by $A(w^{(k)}) \triangleq \frac{\partial \tilde{\nabla} f(w^{(k)})}{\partial w^{(k)}} = \begin{bmatrix} -\nabla_{\phi\phi}^2 f(w^{(k)}) & \nabla_{\phi\theta}^2 f(w^{(k)}) \\ -\nabla_{\theta\phi}^2 f(w^{(k)}) & \nabla_{\theta\theta}^2 f(w^{(k)}) \end{bmatrix}$. In the next, we will replace $A(w^{(k)})$ by A for brevity.

Theorem 1. *For any point within $B_\delta(w^*)$, the Jacobian A in the simple vanilla GAN example trained via SimGD has the following eigenvalues: $\lambda_{1,2}(A) = \frac{-\sigma^2 \pm \sqrt{(\sigma^2)^2 - 4}}{4}$ and $\lambda_{3,4}(A) = \frac{-\beta^2 \pm \sqrt{(\beta^2)^2 - 4}}{4}$ where $\beta^2 \triangleq \sigma^2 + \|v\|^2$.*

Proof: See Appendix A.2. \square

The above theorem shows that $\text{Re}\{\lambda_{1,2}(A)\} < 0$ and $\text{Re}\{\lambda_{3,4}(A)\} < 0$, and thus the SimGD updates in this simple GAN example is asymptotically locally convergent, which is consistent with [13]. Next, we discuss lower bounds of the non-asymptotic convergence rate in two cases.

On the one hand, since we know the variance satisfies $0 < \sigma^2 < 2$, then $\lambda_{1,2}(A)$ are complex eigenvalues. Denote by $\zeta \triangleq \left| \frac{\text{Im}\{\lambda_{1,2}(A)\}}{\text{Re}\{\lambda_{1,2}(A)\}} \right|$ the absolute value of the imaginary-to-real ratio of $\lambda_{1,2}(A)$. The non-asymptotic convergence property determined by $\lambda_{1,2}(A)$ is given as follows.

Corollary 1. *To ensure non-asymptotic local convergence, the step size should satisfy $0 < \eta < \frac{4}{\sqrt{1+\zeta^2}}$. The number of iterations to achieve an ϵ -error solution satisfies $N \geq \frac{2 \log \frac{C_0}{\epsilon}}{\log(1+\frac{1}{\zeta^2})}$ where C_0 is a constant. Specifically, as $\zeta \rightarrow \infty$, N will be at least $O(\zeta^2 \log \frac{1}{\epsilon})$.*

Proof: See Appendix A.3. \square

It shows that when the absolute value of the imaginary-to-real ratio ζ increases, the number of iterations N for a certain convergence performance increases (quadratically in the limit). Since we know $\zeta = \sqrt{(\frac{2}{\sigma^2})^2 - 1}$ in the simple vanilla GAN example, if we assume the variance $\sigma^2 = 0.01$, then $\zeta \approx 200$ and thus $N \geq O(10^4 \log \frac{1}{\epsilon})$ which is apparently too large for such a simple task.

On the other hand, since by assumption we know $\beta^2 > 2$, then $\lambda_{3,4}(A)$ are real eigenvalues. Without loss of generality, we assume $|\lambda_3(A)| \geq |\lambda_4(A)|$ and their ratio is denoted by $\tau \triangleq \left| \frac{\lambda_3(A)}{\lambda_4(A)} \right|$. Thus, τ is a lower bound of the condition number of the Jacobian. The non-asymptotic convergence property determined by $\lambda_{3,4}(A)$ is given as follows.

Corollary 2. *To ensure non-asymptotic local convergence, the step size should also satisfy $0 < \eta < \frac{4}{\sqrt{\tau}}$. For $\tau > 2$, the number of iterations N to achieve an ϵ -error solution satisfies $N > \frac{\log \frac{\epsilon}{C_1}}{\log(1-\frac{2}{\tau})}$ where C_1 is a constant. Specifically, as $\tau \rightarrow \infty$, N will be at least $O(\tau \log \frac{1}{\epsilon})$.*

Proof: See Appendix A.4. \square

It shows that when the lower bound of the condition number τ increases, the number of iterations N for a certain convergence performance guarantee also increases (linearly in the limit). Since we know $\tau = \frac{1}{4}(\beta^2 + \sqrt{(\beta^2)^2 - 4})^2$ in the simple vanilla GAN example, if we assume the norm of the mean $\|v\| = 10$, then $\tau \approx 10^4$ and thus $N \geq O(10^4 \log \frac{1}{\epsilon})$ which also results in a poor convergence rate for such a simple task.

In summary, there exist at least two factors of the Jacobian that can cause the GAN training issues.

- *Phase Factor:* The Jacobian A has complex eigenvalues with a large imaginary-to-real ratio, which has also been reported in [15].
- *Conditioning Factor:* The Jacobian A is ill-conditioned, i.e., the largest absolute value of its eigenvalues is much larger than the smallest one.

Therefore, the GANs with a good convergence behavior should avoid these two factors simultaneously. To this end, Theorem 1 reveals that in the simple GAN example (3), both σ^2 and β^2 should not be too small or too large, which is a relatively strict requirement. Furthermore, changing the expressive power of the generator or discriminator may not easily alleviate these two factors simultaneously. Please see Appendix B for an example of changing the discriminator representations. It might partly explain why GANs trained via SimGD only converge for a very limited set of GAN architectures [5].

4 Jacobian Regularization

A straightforward method to alleviate the above two factors simultaneously is to introduce a *regularization matrix* Γ such that the training updates in (6) become $w^{(k+1)} = w^{(k)} + \eta \Gamma \tilde{\nabla} f(w^{(k)})$ and thus the (regularized) Jacobian is given by $A = \Gamma \frac{\partial \tilde{\nabla} f(w^{(k)})}{\partial w^{(k)}}$. Our goal is to find a specific regularization matrix Γ such that we can appropriately control the eigenvalues of the Jacobian near the equilibrium.

4.1 Revisiting previous methods

There are several gradient-based regularization methods that have been proposed to deal with the training instabilities of GANs from the perspective of controlling Jacobian. First, to overcome the non-convergence issue of training WGAN via SimGD, [13] has proposed to only regularize the generator by using the gradient of the discriminator and the regularized updates are

$$\phi^{(k+1)} = \phi^{(k)} - \eta \nabla_\phi f(w^{(k)}) - \frac{1}{2} \eta \gamma \nabla_\phi \left\| \nabla_\theta f(w^{(k)}) \right\|^2 \quad (7)$$

where the corresponding regularization matrix is $\Gamma = \begin{bmatrix} I & -\gamma \nabla_{\phi\theta}^2 f(w^{(k)}) \\ 0 & I \end{bmatrix}$ with γ being a tunable hyperparameter. Another similar idea is to apply the gradient-based regularization only on the discriminator, called *smoothing optimizer* [15] and the regularized updates are

$$\theta^{(k+1)} = \theta^{(k)} + \eta \nabla_{\theta} f(w^{(k)}) - \frac{1}{2} \eta \gamma \nabla_{\theta} \left\| \nabla_{\phi} f(w^{(k)}) \right\|^2 \quad (8)$$

where the corresponding regularization matrix is $\Gamma = \begin{bmatrix} I & 0 \\ \gamma \nabla_{\theta\phi}^2 f(w^{(k)}) & I \end{bmatrix}$. Furthermore, to alleviate the impact of the *Phase Factor* alone, [15] has proposed ConOpt and the regularized updates are

$$w^{(k+1)} = w^{(k)} + \eta \tilde{\nabla} f(w^{(k)}) - \frac{1}{2} \eta \gamma \nabla \left\| \nabla f(w^{(k)}) \right\|^2 \quad (9)$$

where the corresponding regularization matrix is $\Gamma = \begin{bmatrix} I + \gamma \nabla_{\phi\phi}^2 f(w^{(k)}) & -\gamma \nabla_{\phi\theta}^2 f(w^{(k)}) \\ \gamma \nabla_{\theta\phi}^2 f(w^{(k)}) & I - \gamma \nabla_{\theta\theta}^2 f(w^{(k)}) \end{bmatrix}$.

Their behaviors in terms of stabilizing the simple vanilla GAN example (3) are given as follows.

Theorem 2. *In the simple vanilla GAN example above, none of the gradient-based regularization methods (only regularizing generator, smoothing optimizer and ConOpt) are capable of simultaneously alleviating the Phase Factor and Conditioning Factor.*

Proof: See Appendix D.1. \square

From the above theorem, together with the example of changing the representations in Appendix B, we can see that without careful considerations of both the *Phase Factor* and *Conditioning Factor*, these GAN variants might still suffer from poor convergence even in the simple GAN example.

4.2 JR-GAN

Based on the previous methods, we propose a new but simple Jacobian regularization, called JR-GAN, which also applies the regularization terms based on the gradients of the generator and discriminator. Specifically, the regularized updates are given by

$$\begin{aligned} \phi^{(k+1)} &= \phi^{(k)} - \eta \nabla_{\phi} f(w^{(k)}) - \frac{1}{2} \eta \gamma \nabla_{\phi} \left\| \nabla_{\theta} f(w^{(k)}) \right\|^2 \\ \theta^{(k+1)} &= \theta^{(k)} + \eta \nabla_{\theta} f(w^{(k)}) - \frac{1}{2} \eta \gamma \nabla_{\theta} \left\| \nabla_{\phi} f(w^{(k)}) \right\|^2 \end{aligned} \quad (10)$$

Similarly, $\gamma > 0$ is a tunable parameter, and we can get the corresponding regularization matrix as $\Gamma = \begin{bmatrix} I & -\gamma \nabla_{\phi\theta}^2 f(w^{(k)}) \\ \gamma \nabla_{\theta\phi}^2 f(w^{(k)}) & I \end{bmatrix}$. Note that the key difference between the updates of

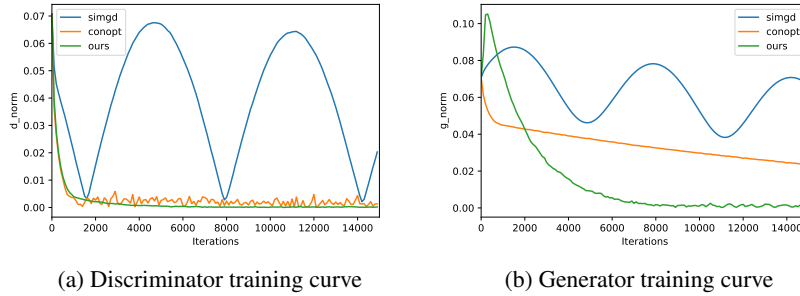
JR-GAN in (10) and ConOpt in (9) is that JR-GAN does not introduce the Hessians $\nabla_{\phi\phi}^2 f(w^{(k)})$ and $\nabla_{\theta\theta}^2 f(w^{(k)})$ in the regularization matrix Γ . Intuitively, a reason for doing this is to avoid the risk of reversing the gradient flows, which might damage the GAN training (see Appendix C for a detailed explanation). The following theorem shows the eigenvalues of the Jacobian for the simple vanilla GAN dynamics trained via our proposed regularization.

Theorem 3. *For any point within $B_{\delta}(w^*)$, the Jacobian A in the simple vanilla GAN example trained via the JR-GAN updates (10) has the following eigenvalues: $\lambda_{1,2}(A) = \frac{-(\sigma^2 + \gamma) \pm \sqrt{(\sigma^2 + \gamma)^2 - (\gamma^2 + 4)}}{4}$ and $\lambda_{3,4}(A) = \frac{-(\beta^2 + \gamma) \pm \sqrt{(\beta^2 + \gamma)^2 - (\gamma^2 + 4)}}{4}$, where $\beta^2 \triangleq \sigma^2 + \|v\|^2$.*

Proof: See Appendix D.2. \square

From the above theorem, we can evaluate both $\zeta \triangleq \left| \frac{\text{Im}\{\lambda_{1,2}(A)\}}{\text{Re}\{\lambda_{1,2}(A)\}} \right|$ and $\tau \triangleq \left| \frac{\lambda_3(A)}{\lambda_4(A)} \right|$, two key variables that reflect the impact of the *Phase Factor* and *Conditioning Factor*, respectively, and see how the tunable parameter γ in JR-GAN changes their values. The results are given in the following corollary.

Corollary 3. *In the simple vanilla GAN example trained via (10), ζ monotonically decreases with γ , and if $\gamma \geq 2$, then τ also monotonically decreases with γ . In the limit of $\gamma \rightarrow \infty$, we get $\zeta \rightarrow 0$ (i.e., no complex eigenvalues) and $\tau \rightarrow 1$ (i.e., well conditioned). Therefore, we can make γ large enough in JR-GAN to alleviate the impact of the Phase Factor and Conditioning Factor simultaneously.*



(a) Discriminator training curve

(b) Generator training curve

Figure 1: Training dynamics of SimGD, ConOpt and JR-GAN (Ours) in the simple vanilla GAN example where $\mu = 4$ and $\sigma^2 = 0.04$. (a) shows the discriminator convergence where “d_norm” denotes the l_2 distance between the current and optimal value of the discriminator parameters, and (b) shows the generator convergence where “g_norm” denotes the l_2 distance between the current and optimal value of the generator parameters.

Proof. See Appendix D.3. \square

According to Corollary 1 and 2, if $\zeta \rightarrow 0$ and $\tau \rightarrow 1$, the non-asymptotic convergence performance will be improved greatly. Therefore, the above corollary theoretically shows that our proposed method JR-GAN could provide a good local convergence behavior by tuning the hyperparameter γ . Note that even so, we cannot make γ arbitrarily large in JR-GAN. According to the non-asymptotic analysis, the step size should also satisfy $0 < \eta < \eta_{\max}$ where $\eta_{\max} \triangleq 8 \min\{\frac{\gamma+\sigma^2}{\gamma^2+4}, \frac{1}{(\beta^2+\gamma)+\sqrt{2\beta^2\gamma+(\beta^2)^2-4}}\}$. As we can see η_{\max} decreases with the increment of γ , and goes to 0 as $\gamma \rightarrow \infty$. So when γ is sufficiently large, we have to make the step size infinitely small accordingly.

5 Experiments

Isotropic Gaussian. First, we empirically verify our theory in the simple vanilla GAN example. Specifically, we consider a two-dimensional case, i.e. $n = 2$ and the mean of true data is $v = [0, \mu]^T$. To test the local convergence, the parameters of both the discriminator and generator are initialized within $B_\delta(w^*)$ where $\delta = 0.05$. Unless stated otherwise, we set the learning rate to be $\eta = 0.001$, the regularization parameter to be $\gamma = 10$, the optimizer to be the stochastic gradient descent (SGD) with a batch size 128, and run 15K iterations.

Figure 1 shows the discriminator and generator training curves, respectively, for three training methods: SimGD, ConOpt and JR-GAN (Ours) by letting $\mu = 4$ and $\sigma^2 = 0.04$. We observe that for SimGD, the training curves oscillate with very weak damping which becomes even weaker if we increase μ or decrease σ^2 (See Figures 5 and 6 in Appendix E.1). It verifies that SimGD might suffer from poor convergence caused by the *Phase Factor* and *Conditioning Factor*. Also, ConOpt could alleviate the *Phase Factor* since oscillations caused by complex eigenvalues disappear. However, its generator convergence is heavily slowed down by the *Conditioning Factor* which becomes worse as we increase μ (See Figure 5 in Appendix E.1). In contrast, the JR-GAN enjoys a decent convergence rate for both the generator and discriminator by alleviating the two factors simultaneously.

Mixture of Gaussians. Second, we test JR-GAN in a commonly used toy example where the goal is to learn a mixture of Gaussians with modes uniformly distributed around a circle with radius r . We note that ConOpt does much better than SimGD in this toy example with $r = 1$ [15]. Here we make the task harder by letting $r = 10$ while keeping other settings the same with [15]. The generator and discriminator are both fully connected neural networks with 4 hidden layers and 256 units for each hidden layer. We run SimGD, ConOpt and JR-GAN (Ours) with RMSProp [19] and learning rate of 10^{-4} for 10K iterations, and the input noise is sampled from a 64-dimensional Gaussian $\mathcal{N}(0, rI_{64})$. Experimentally, we find $\gamma = 10$ works best for ConOpt while $\gamma = 1000$ works best for JR-GAN.

Figure 2 shows the results of SimGD, ConOpt and JR-GAN (Ours) over different iterations. We can see that SimGD still oscillates among different modes and fails to converge, while ConOpt converges to some suboptimal solution. Only JR-GAN is able to converge to the target data distribution. Please see Figures 7 and 8 in Appendix E.1 for more detailed comparison among these three methods.

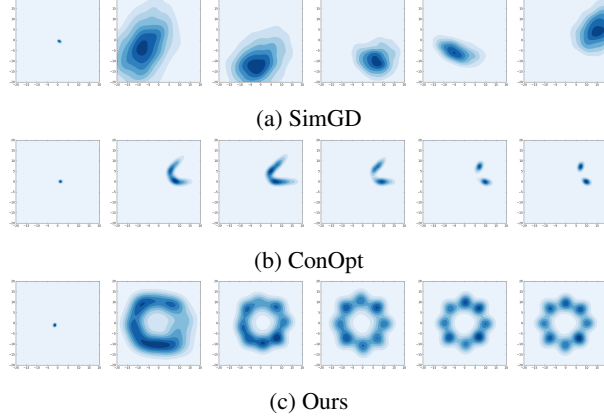


Figure 2: Comparison of SimGD, ConOpt and JR-GAN (Ours) on the mixture of Gaussians over iterations where $r = 10$. From left to right, each row consists of the results after 0, 2000, 4000, 6000, 8000 and 10000 iterations. Note that here we choose $\gamma = 10$ for ConOpt and $\gamma = 1000$ for JR-GAN.

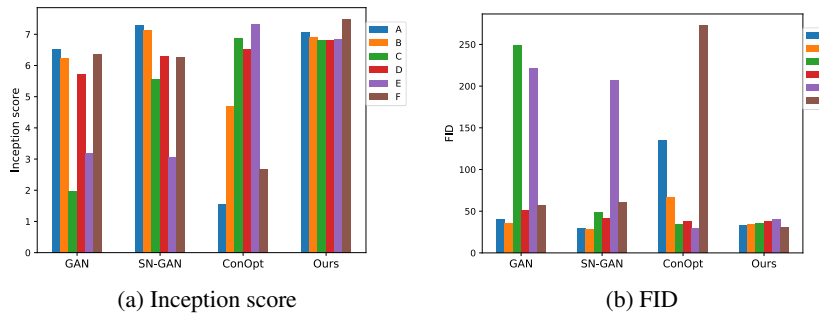


Figure 3: Inception scores and FIDs of different training methods with different GAN settings on the CIFAR-10 dataset. For inception score, the higher is better. For FID, the lower is better.

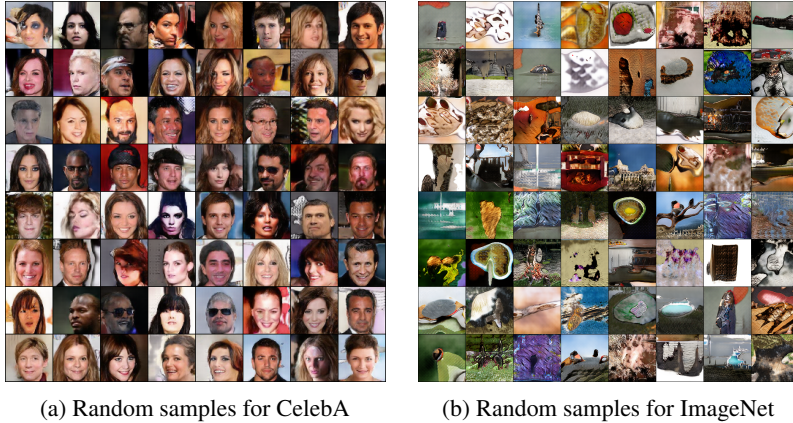
CIFAR-10. In this experiment, we quantitatively evaluate the sample quality of JR-GAN on the CIFAR-10 dataset [20] by applying the *inception score* [6] and *Frechet inception distance* (FID) [16]. First, we test the dependencies of JR-GAN on different network architectures and hyperparameters. We also compare with other GAN training methods, including the standard GAN via the alternative gradient descent [1] (denoted as ‘GAN’), ConOpt and SN-GAN [11]. For all methods, we use the non-saturating loss as suggested in [1]. For fair comparison, we test 6 settings: the standard CNN model in [11] with batch normalization [21] on generator (A) or without batch normalization on generator (B), the DCGAN-like architecture with a constant number of filters in [15] via the Adam optimizer [22] (C) or via the RMSProp optimizer (D), and the ResNet [23] architectures v1 (E) or v2 (F) with a constant number of filters. Note that the first four settings (A-D) are based on the architectures used in the previous works. Please refer to Table 2 and 3 in Appendix E.2 for the architectures E and F where $M_f = 64$. Unless otherwise stated, we use the Adam optimizer with $\beta_1 = 0.5$ and $\beta_2 = 0.999$. Also, we use a batch size of 64 and run all experiments with a learning rate of 10^{-4} for 500K iterations. For ConOpt, we set $\gamma = 10$, and for JR-GAN, we set $\gamma = 100$.

Figure 3 shows the inception score and FID results for different training methods with all 6 settings on CIFAR-10. We can see that JR-GAN is more robust than other methods with respect to different network architectures and hyperparameters. Both SN-GAN and ConOpt perform almost the best in their own proposed GAN architectures but perform poorly in other cases. In addition, we compare JR-GAN with multiple state-of-the-art GAN models in Table 1. Please see Table 3 in Appendix E.2 for the detailed network architectures where we set $M_f = 256$ and use a learning rate of 5×10^{-5} for better scores. We can see that JR-GAN outperforms SN-GAN in terms of both inception score and FID, and also achieves the near state-of-the-art results with a relatively low computational complexity.

CelebA and ImageNet. In this experiment, we qualitatively evaluate the generated samples of JR-GAN on the CelebA (with size of 64×64) [28] and ILSVRC2012 (ImageNet, with size of

| Method | Inception score | FID |
|--------------|----------------------------------|----------------------------------|
| Real data | $11.24 \pm .12$ | 7.8 |
| DCGAN [5] | $6.64 \pm .14$ | 34.3^\dagger |
| LR-GAN [24] | $7.17 \pm .07$ | - |
| DFM [25] | $7.72 \pm .13$ | 30.1^\dagger |
| WGAN-GP [9] | $7.86 \pm .08$ | 28.2^\dagger |
| SN-GAN [11] | $8.22 \pm .05$ | $21.7 \pm .21$ |
| OT-GAN* [26] | $8.47 \pm .12$ | - |
| PG-GAN* [27] | $8.56 \pm .06$ | 19.1^\dagger |
| Ours | $8.35 \pm .08$ | $19.9 \pm .96$ |

Table 1: Inception scores and FIDs on CIFAR-10 where all methods are trained in an unsupervised manner. For our results, we train the same architecture for 10 times with different random seeds and calculate the mean and standard derivation after 500K iterations. Note that models marked by * require large amounts of computation as they either use a very large batch size [26] or apply the multi-scale training [27]. Also just for reference, the FIDs marked by \dagger are obtained from <https://github.com/pfnet-research/chainer-gan-lib> with only one trial.



(a) Random samples for CelebA (b) Random samples for ImageNet

Figure 4: Random samples generated by JR-GANs trained on CelebA and ImageNet, respectively, in an unsupervised manner. For CelebA, the sample size is 64×64 , and for ImageNet, the sample size is 128×128 .

128×128) [29] datasets. Due to the limitation of our computational budgets, we do not apply large hyperparameter searches. Instead, we use a similar training setup as for the CIFAR-10 experiments, with slightly different network architectures. Please see Tables 4 and 5 in Appendix E.2 for details.

Figure 4 (a) and (b) show the randomly generated samples of JR-GAN trained on CelebA and ImageNet, respectively. We can see that for CelebA, JR-GAN can produce realistic and diverse celebrity faces (also with various backgrounds). For ImageNet, JR-GAN can stabilize the training well while other training methods quickly collapse. While not completely realistic, it can generate visually convincing and diverse images from 1000 ImageNet classes in a completely unsupervised manner. The good results of JR-GAN on CelebA and ImageNet demonstrate its ability of stabilizing the GAN training on more complex tasks.

6 Conclusions

In this paper, we analyzed the non-asymptotic local convergence behavior of the GAN training dynamics in a simple GAN example. We found out that to ensure a good convergence behavior, both the *Phase Factor* and *Conditioning Factor* should be alleviated simultaneously, but previous gradient-based regularizations can only avoid one factor while making the other more severe. Therefore, we proposed a new Jacobian regularization method, called JR-GAN, and in theory showed it can alleviate the two factors simultaneously. Finally, we did extensive experiments to show the training stability and sample quality of JR-GAN. In the future, we would like to further improve the sample quality of JR-GAN on complex datasets, such as ImageNet. Besides, we believe there exist more efficient Jacobian regularization methods based on our theoretical analysis.

References

- [1] I. Goodfellow, J. Pouget-Abadie, M. Mirza, B. Xu, D. Warde-Farley, S. Ozair, A. Courville, and Y. Bengio, “Generative adversarial nets,” in *Advances in neural information processing systems (NIPS)*, pp. 2672–2680, 2014.
- [2] J. Ho and S. Ermon, “Generative adversarial imitation learning,” in *Advances in Neural Information Processing Systems (NIPS)*, pp. 4565–4573, 2016.
- [3] J.-Y. Zhu, T. Park, P. Isola, and A. A. Efros, “Unpaired image-to-image translation using cycle-consistent adversarial networks,” in *Proceedings of the IEEE Conference on Computer Vision and Pattern Recognition (CVPR)*, pp. 2223–2232, 2017.
- [4] C. Ledig, L. Theis, F. Huszar, J. Caballero, A. Cunningham, A. Acosta, A. Aitken, A. Tejani, J. Totz, Z. Wang, *et al.*, “Photo-realistic single image super-resolution using a generative adversarial network,” in *Proceedings of the IEEE Conference on Computer Vision and Pattern Recognition (CVPR)*, pp. 4681–4690, 2017.
- [5] A. Radford, L. Metz, and S. Chintala, “Unsupervised representation learning with deep convolutional generative adversarial networks,” *arXiv preprint arXiv:1511.06434*, 2015.
- [6] T. Salimans, I. Goodfellow, W. Zaremba, V. Cheung, A. Radford, and X. Chen, “Improved techniques for training gans,” in *Advances in Neural Information Processing Systems (NIPS)*, pp. 2234–2242, 2016.
- [7] S. Nowozin, B. Cseke, and R. Tomioka, “f-gan: Training generative neural samplers using variational divergence minimization,” in *Advances in Neural Information Processing Systems (NIPS)*, pp. 271–279, 2016.
- [8] M. Arjovsky, S. Chintala, and L. Bottou, “Wasserstein generative adversarial networks,” in *International Conference on Machine Learning (ICML)*, pp. 214–223, 2017.
- [9] I. Gulrajani, F. Ahmed, M. Arjovsky, V. Dumoulin, and A. C. Courville, “Improved training of wasserstein gans,” in *Advances in Neural Information Processing Systems (NIPS)*, pp. 5769–5779, 2017.
- [10] K. Roth, A. Lucchi, S. Nowozin, and T. Hofmann, “Stabilizing training of generative adversarial networks through regularization,” in *Advances in Neural Information Processing Systems (NIPS)*, pp. 2015–2025, 2017.
- [11] T. Miyato, T. Kataoka, M. Koyama, and Y. Yoshida, “Spectral normalization for generative adversarial networks,” in *ICLR*, 2018.
- [12] I. Goodfellow, “Nips 2016 tutorial: Generative adversarial networks,” *arXiv preprint arXiv:1701.00160*, 2016.
- [13] V. Nagarajan and J. Z. Kolter, “Gradient descent gan optimization is locally stable,” in *Advances in Neural Information Processing Systems (NIPS)*, pp. 5591–5600, 2017.
- [14] L. Mescheder, A. Geiger, and S. Nowozin, “Which training methods for gans do actually converge?,” *arXiv preprint arXiv:1801.04406*, 2018.
- [15] L. Mescheder, S. Nowozin, and A. Geiger, “The numerics of gans,” in *Advances in Neural Information Processing Systems (NIPS)*, pp. 1823–1833, 2017.
- [16] M. Heusel, H. Ramsauer, T. Unterthiner, B. Nessler, and S. Hochreiter, “Gans trained by a two time-scale update rule converge to a local nash equilibrium,” in *Advances in Neural Information Processing Systems (NIPS)*, pp. 6629–6640, 2017.
- [17] D. Arrowsmith and C. M. Place, *Dynamical systems: differential equations, maps, and chaotic behaviour*, vol. 5. CRC Press, 1992.
- [18] A. Yadav, S. Shah, Z. Xu, D. Jacobs, and T. Goldstein, “Stabilizing adversarial nets with prediction methods,” in *ICLR*, 2018.

- [19] T. Tieleman and G. Hinton, “Lecture 6.5—rmsprop: Divide the gradient by a running average of its recent magnitude,” 2012.
- [20] A. Torralba, R. Fergus, and W. T. Freeman, “80 million tiny images: A large data set for nonparametric object and scene recognition,” *IEEE transactions on pattern analysis and machine intelligence*, vol. 30, no. 11, pp. 1958–1970, 2008.
- [21] S. Ioffe and C. Szegedy, “Batch normalization: Accelerating deep network training by reducing internal covariate shift,” *arXiv preprint arXiv:1502.03167*, 2015.
- [22] D. P. Kingma and J. Ba, “Adam: A method for stochastic optimization,” in *ICLR*, 2015.
- [23] K. He, X. Zhang, S. Ren, and J. Sun, “Deep residual learning for image recognition,” in *Proceedings of the IEEE conference on computer vision and pattern recognition (CVPR)*, pp. 770–778, 2016.
- [24] J. Yang, A. Kannan, D. Batra, and D. Parikh, “Lr-gan: Layered recursive generative adversarial networks for image generation,” *arXiv preprint arXiv:1703.01560*, 2017.
- [25] D. Warde-Farley and Y. Bengio, “Improving generative adversarial networks with denoising feature matching,” in *ICLR*, 2016.
- [26] T. Salimans, H. Zhang, A. Radford, and D. Metaxas, “Improving gans using optimal transport,” in *ICLR*, 2018.
- [27] T. Karras, T. Aila, S. Laine, and J. Lehtinen, “Progressive growing of gans for improved quality, stability, and variation,” in *ICLR*, 2018.
- [28] Z. Liu, P. Luo, X. Wang, and X. Tang, “Deep learning face attributes in the wild,” in *Proceedings of International Conference on Computer Vision (ICCV)*, 2015.
- [29] O. Russakovsky, J. Deng, H. Su, J. Krause, S. Satheesh, S. Ma, Z. Huang, A. Karpathy, A. Khosla, M. Bernstein, *et al.*, “Imagenet large scale visual recognition challenge,” *International Journal of Computer Vision*, vol. 115, no. 3, pp. 211–252, 2015.

A Proofs in Section 3

A.1 Proof of Lemma 1

Proof. First, we have

$$\nabla_\phi f(\phi, \theta) = \mathbb{E}_{z \sim \mathcal{N}(0, \sigma^2 I)} [g'_2(\theta^T(\phi + z))\theta]$$

Since the equilibrium point (ϕ^*, θ^*) satisfies $\theta^{*T}(\phi^* + z) = 0$, for points (ϕ, θ) near the equilibrium, we know $g'_2(\theta^T(\phi + z)) = g'_2(0) + g''_2(0)\theta^T(\phi + z) + o(\|\theta\|)$ by Taylor expansion. That is, by ignoring the small term with norm $o(\|\theta\|)$, we have

$$\begin{aligned} \nabla_\phi f(\phi, \theta) &\approx \mathbb{E}_{z \sim \mathcal{N}(0, \sigma^2 I)} [g'_2(0)\theta + g''_2(0)\theta\theta^T(\phi + z)] \\ &= g'_2(0)\theta + g''_2(0)\theta\theta^T\phi \\ &\stackrel{(a)}{\approx} g'_2(0)\theta \end{aligned}$$

where (a) is also from ignoring the small term with norm $o(\|\theta\|)$. Similarly,

$$\begin{aligned} \nabla_\theta f(\phi, \theta) &= \mathbb{E}_{x \sim \mathcal{N}(v, \sigma^2 I)} [g'_1(\theta^T x)x] + \mathbb{E}_{\tilde{x} \sim \mathcal{N}(\phi, \sigma^2 I)} [g'_2(\theta^T \tilde{x})\tilde{x}] \\ &\stackrel{(a)}{\approx} \mathbb{E}_{x \sim \mathcal{N}(v, \sigma^2 I)} [(g'_1(0) + g''_1(0)\theta^T x)x] + \mathbb{E}_{\tilde{x} \sim \mathcal{N}(\phi, \sigma^2 I)} [(g'_2(0) + g''_2(0)\theta^T \tilde{x})\tilde{x}] \\ &= g'_1(0)v + g''_1(0)(\sigma^2 I + vv^T)\theta + g'_2(0)\phi + g''_2(0)(\sigma^2 I + \phi\phi^T)\theta \\ &\stackrel{(b)}{\approx} g'_1(0)v + g'_2(0)\phi + (g''_1(0) + g''_2(0))(\sigma^2 I + vv^T)\theta \end{aligned}$$

where (a) is from $g'_1(\theta^T x) = g'_1(0) + g''_1(0)\theta^T x + o(\|\theta\|)$ and $g'_2(\theta^T \tilde{x}) = g'_2(0) + g''_2(0)\theta^T \tilde{x} + o(\|\theta\|)$ by Taylor expansion, and (b) is from $\|\phi - v\| = o(1)$.

For second-order derivatives, we have

$$\begin{aligned} \nabla_{\phi\phi}^2 f(\phi, \theta) &= \mathbb{E}_{z \sim \mathcal{N}(0, \sigma^2 I)} [g''_2(\theta^T(\phi + z))\theta\theta^T] \\ &\stackrel{(a)}{\approx} g''_2(0)\theta\theta^T \end{aligned}$$

where (a) also follows from $g''_2(\theta^T(\phi + z)) = g''_2(0) + o(1)$ by Taylor expansion. Also,

$$\begin{aligned} \nabla_{\theta\phi}^2 f(\phi, \theta) &= \mathbb{E}_{\tilde{x} \sim \mathcal{N}(\phi, \sigma^2 I)} [g'_2(\theta^T \tilde{x})I + g''_2(\theta^T \tilde{x})\tilde{x}\theta^T] \\ &\stackrel{(a)}{\approx} \mathbb{E}_{\tilde{x} \sim \mathcal{N}(\phi, \sigma^2 I)} [(g'_2(0) + g''_2(0)\theta^T \tilde{x})I + g''_2(0)\tilde{x}\theta^T] \\ &= g'_2(0)I + g''_2(0)\theta^T\phi I + g''_2(0)\phi\theta^T \\ &\stackrel{(b)}{\approx} g'_2(0)I \end{aligned}$$

where (a) is from $g'_2(\theta^T \tilde{x}) = g'_2(0) + g''_2(0)\theta^T \tilde{x} + o(\|\theta\|)$ and $g''_2(\theta^T \tilde{x}) = g''_2(0) + o(1)$ by Taylor expansion, and (b) is from $\|\theta\| = o(1)$, and

$$\begin{aligned} \nabla_{\theta\theta}^2 f(\phi, \theta) &= \mathbb{E}_{x \sim \mathcal{N}(v, \sigma^2 I)} [g''_1(\theta^T x)xx^T] + \mathbb{E}_{\tilde{x} \sim \mathcal{N}(\phi, \sigma^2 I)} [g''_2(\theta^T \tilde{x})\tilde{x}\tilde{x}^T] \\ &\stackrel{(a)}{\approx} \mathbb{E}_{x \sim \mathcal{N}(v, \sigma^2 I)} [g''_1(0)xx^T] + \mathbb{E}_{\tilde{x} \sim \mathcal{N}(\phi, \sigma^2 I)} [g''_2(0)\tilde{x}\tilde{x}^T] \\ &\stackrel{(b)}{\approx} (g''_1(0) + g''_2(0))(\sigma^2 I + vv^T) \end{aligned}$$

where (a) is from $g''_1(\theta^T x) = g''_1(0) + o(1)$ and $g''_2(\theta^T \tilde{x}) = g''_2(0) + o(1)$ by Taylor expansion, and (b) is from $\|\phi - v\| = o(1)$. \square

A.2 Proof of Theorem 1

Proof. For the vanilla GAN, we know $g_1(t) = g_2(-t) = -\log(1 + e^{-t})$. Then we have $g'_1(0) = \frac{1}{2}$, $g'_2(0) = -\frac{1}{2}$ and $g''_1(0) = g''_2(0) = -\frac{1}{4}$. From Lemma 1, the updates (6) of SimGD near the

equilibrium w^* becomes

$$\begin{aligned} w^{(k+1)} &= w^{(k)} + \eta \left[\frac{1}{2}(\phi^{(k)} - v) + \frac{1}{2}(\sigma^2 I + vv^T) \theta^{(k)} \right] \\ &= w^{(k)} + \eta \underbrace{\begin{bmatrix} 0 & \frac{1}{2}I \\ -\frac{1}{2}I & -\frac{1}{2}(\sigma^2 I + vv^T) \end{bmatrix}}_{\triangleq A} w^{(k)} \end{aligned} \quad (11)$$

where $w^{(k)} \triangleq \begin{bmatrix} \phi^{(k)} - v \\ \theta^{(k)} \end{bmatrix}$. Next, we need to compute the eigenvalues of the Jacobian A . By definition, let $Ay = \lambda y$ where the eigenvector satisfies $y = \begin{bmatrix} y_1 \\ y_2 \end{bmatrix} \neq 0$, then we have

$$\frac{1}{2}y_2 = \lambda y_1 \quad (12)$$

$$-\frac{1}{2}y_1 - \frac{1}{2}(\sigma^2 I + vv^T)y_2 = \lambda y_2 \quad (13)$$

First, we know $\lambda \neq 0$, otherwise, we get $y = 0$ which violates the definition of eigenvectors. Thus from (12) we have $y_1 = \frac{1}{2\lambda}y_2$. Plugging it into (13) yields

$$-\lambda vv^T y_2 = (2\lambda^2 + \sigma^2\lambda + \frac{1}{2})y_2 \quad (14)$$

Then we can evaluate λ in two cases:

(1) $v^T y_2 = 0$. From (14) we have $(4\lambda^2 + 2\sigma^2\lambda + 1)y_2 = 0$. Similarly we know $y_2 \neq 0$, otherwise, we get $y_1 = 0$ as well from (13) which again violates the definition of eigenvectors. Thus, the coefficient satisfies $4\lambda^2 + 2\sigma^2\lambda + 1 = 0$, and solving this equation yields $\lambda_{1,2}(A)$ in the theorem.

(2) $v^T y_2 \neq 0$. By left multiplying v^T on both sides of Eq. (14) we get $-\lambda\|v\|^2 v^T y_2 = (2\lambda^2 + \sigma^2\lambda + \frac{1}{2})v^T y_2$. Since $v^T y_2 \neq 0$, we have $4\lambda^2 + 2(\sigma^2 + \|v\|^2)\lambda + 1 = 0$, and solving this equation yields $\lambda_{3,4}(A)$ in the theorem. \square

A.3 Proof of Corollary 1

Proof. In the first part of the proof, we try to find the range of the step size η . Given $\sigma^2 < 2$, we know $\lambda_{1,2}(A)$ are complex eigenvalues and thus $|1 + \eta\lambda_{1,2}(A)| = \frac{1}{4}\eta^2 - \frac{\sigma^2}{2}\eta + 1$. Since it requires $|1 + \eta\lambda_{1,2}(A)| < 1$ to ensure the non-asymptotic convergence, by setting $\frac{1}{4}\eta^2 - \frac{\sigma^2}{2}\eta + 1 < 1$ we get $0 < \eta < 2\sigma^2$. As we know $\zeta = \sqrt{(\frac{\sigma^2}{2})^2 - 1}$ in the simple vanilla GAN example, then $\sigma^2 = \frac{2}{\sqrt{1+\zeta^2}}$, which means $0 < \eta < \frac{4}{\sqrt{1+\zeta^2}}$.

In the second part of the proof, we try to find the lower bound of the number of iterations N given the step size constraint. We know $\frac{1}{4}\eta^2 - \frac{\sigma^2}{2}\eta + 1 \geq \sqrt{1 - (\frac{\sigma^2}{2})^2}$ with the equality holds at $\eta = \sigma^2$. Therefore, for the step size η satisfying $0 < \eta < \frac{4}{\sqrt{1+\zeta^2}}$, we have $\frac{1}{\sqrt{1+\frac{1}{\zeta^2}}} \leq |1 + \eta\lambda_{1,2}(A)| < 1$. Thus, for the updates $w^{(k)} = (I + \eta A)w^{(k-1)}$, it is easy to get $\tilde{w}^{(k)} = (I + \eta\Lambda)\tilde{w}^{(k-1)}$ where the eigen-matrix Λ satisfying $\Lambda = PAP^{-1}$ with P invertible and $\tilde{w}^{(k)} = Pw^{(k)}$. Apparently, $|\tilde{w}_j^{(k)}| = |I + \eta\lambda_{1,2}(A)|^k |\tilde{w}_j^{(0)}|$ where the index j refers to the entry in $\tilde{w}^{(k)}$ related to the eigenvalues $\lambda_{1,2}(A)$. Also, we know $\|\tilde{w}^{(k)}\| \geq |\tilde{w}_j^{(k)}|$ and $\|\tilde{w}^{(k)}\| = \|Pw^{(k)}\| \leq \|P\| \|w^{(k)}\|$, so we have $\|w^{(k)}\| \geq |I + \eta\lambda_{1,2}(A)|^k \|P\|^{-1} |\tilde{w}_j^{(0)}|$. Therefore, for the ϵ -error solution $\|w^{(N)}\| \leq \epsilon$ after N iterations, we have $(1 + \frac{1}{\zeta^2})^{-\frac{N}{2}} \|P\|^{-1} |\tilde{w}_j^{(0)}| \leq \epsilon$. By letting $C_0 = \|P\|^{-1} |\tilde{w}_j^{(0)}|$, we can easily get the lower bound of N . \square

A.4 Proof of Corollary 2

Proof. In the first part of the proof, we try to find the range of the step size η . Given $\beta^2 > 2$, $\lambda_{3,4}(A)$ are both real eigenvalues. Similarly, to ensure the non-asymptotic convergence, the step size

η also satisfies $|1 + \eta\lambda_{3,4}(A)| < 1$. From Theorem 1 we have $1 + \eta\lambda_3(A) = 1 - \frac{\beta^2 + \sqrt{(\beta^2)^2 - 4}}{4}\eta$ and $1 + \eta\lambda_4(A) = 1 - \frac{\beta^2 - \sqrt{(\beta^2)^2 - 4}}{4}\eta$. Next, we analyze $\lambda_3(A)$ and $\lambda_4(A)$ separately. To ensure $|1 + \eta\lambda_3(A)| < 1$, then $0 < \eta < \frac{8}{\beta^2 + \sqrt{(\beta^2)^2 - 4}}$. As we know $\tau = \frac{1}{4}(\beta^2 + \sqrt{(\beta^2)^2 - 4})^2$ in the simple vanilla GAN example, then $\frac{8}{\beta^2 + \sqrt{(\beta^2)^2 - 4}} = \frac{4}{\sqrt{\tau}}$, which means $0 < \eta < \frac{4}{\sqrt{\tau}}$. Also, to satisfy $|1 + \eta\lambda_4(A)| < 1$, then $0 < \eta < 2(\beta^2 + \sqrt{(\beta^2)^2 - 4}) = 4\sqrt{\tau}$. As we know $\tau > 1$ by definition, the step size η satisfies $0 < \eta < \min\{\frac{4}{\sqrt{\tau}}, 4\sqrt{\tau}\} = \frac{4}{\sqrt{\tau}}$.

In the second part of the proof, we try to find the lower bound of the number of iterations N given the step size constraint. We know $|1 + \eta\lambda_4(A)| = |1 - \frac{1}{2\sqrt{\tau}}\eta|$ and for $0 < \eta < \frac{4}{\sqrt{\tau}}$ we get $1 - \frac{2}{\tau} < 1 - \frac{1}{2\sqrt{\tau}}\eta < 1$. Therefore, if $1 < \tau < 2$, then $-1 < 1 - \frac{2}{\tau} < 0$, and thus $0 < |1 + \eta\lambda_4(A)| < 1$. If $\tau \geq 2$, then $1 - \frac{2}{\tau} > 0$, and thus $1 - \frac{2}{\tau} < |1 + \eta\lambda_4(A)| < 1$. Putting them together, we get $\max\{1 - \frac{2}{\tau}, 0\} < |1 + \eta\lambda_4(A)| < 1$. Similar to the proof of Corollary 1, we rewrite the updates as $\tilde{w}^{(k)} = (I + \eta\Lambda)\tilde{w}^{(k-1)}$ where the eigen-matrix Λ satisfying $\Lambda = PAP^{-1}$ with P invertible and $\tilde{w}^{(k)} = Pw^{(k)}$. Here we focus on $|\tilde{w}_{j'}^{(k)}| = |I + \eta\lambda_{1,2}(A)|^k |\tilde{w}_{j'}^{(0)}|$ where the index j' refers to the entry in $\tilde{w}^{(k)}$ related to the eigenvalues $\lambda_4(A)$. Also, we know $\|w^{(k)}\| \geq |I + \eta\lambda_{1,2}(A)|^k C_1$ where $C_1 = \|P\|^{-1} |\tilde{w}_{j'}^{(0)}|$. Therefore, for $\tau > 2$, we get $\|w^{(k)}\| \geq (1 - \frac{2}{\tau})^{\frac{k}{2}} C_1$. For the ϵ -error solution $\|w^{(N)}\| \leq \epsilon$, we have $(1 - \frac{2}{\tau})^{\frac{N}{2}} C_1 \leq \epsilon$ which yields the lower bound of N . \square

B An example of full rank representations

In the simple vanilla GAN example, if we consider the zero noise-limit case, i.e. $\sigma^2 = 0$, and assume $n = 1$, from Theorem 1 we know the eigenvalues of the Jacobian A are

$$\lambda_{1,2}(A) = \frac{-v^2 \pm \sqrt{(v^2)^2 - 4}}{4} \quad (15)$$

When $v \rightarrow 0$, $\lambda_{1,2}(A) \rightarrow \pm \frac{1}{2}i$ with an infinitely large imaginary-to-real ratio ζ , which obviously suffers from the impact of the *Phase Factor*.

To alleviate this issue, one solution could be to increase the expressive power of discriminator. For instance, it is suggested by [14] that we can replace the linear discriminator $D_\theta(x) = \theta x$ by the discriminator with the so-called full-rank representations $D_\theta(x) = \theta e^x$. Similarly, in the zero noise-limit case with $n = 1$, we first rewrite the objective (3) as $f(\theta, \phi) = g_1(\theta e^x) + g_2(-\theta e^x)$. For the vanilla GAN, we have $g_1(t) = g_2(-t) = -\log(1 + e^{-t})$. Then the Jacobian A of all points within $B_\delta(w^*)$ is evaluated as $A = \begin{bmatrix} 0 & \frac{1}{2}e^v \\ -\frac{1}{2}e^v & -\frac{1}{2}e^{2v} \end{bmatrix}$ and its eigenvalues are

$$\lambda_{1,2}(A) = \frac{-e^{2v} \pm \sqrt{e^{4v} - 4e^{2v}}}{4} \quad (16)$$

Now when $v \rightarrow 0$, $\lambda_{1,2}(A) \rightarrow \frac{-1 \pm \sqrt{3}i}{4}$ with the imaginary-to-real ratio $\zeta = \sqrt{3}$. By Corollary 1, the impact of the *Phase Factor* has been effectively alleviated when v is very small.

However, the impact of the *Conditioning Factor*, if it exists, becomes much more severe. Asymptotically when v is sufficiently large, from (15) we know that τ increases in the order of v^4 , but (16) shows that τ increases in the order of e^{2v} . For example, if we assume $v = 5$, the eigenvalues of the original Jacobian (15) is evaluated as $\lambda_{1,2}(A) = \frac{-25 \pm \sqrt{625}}{2}$ with $\tau = \Omega(10^2)$. However, after using the discriminator with full-rank representations, the eigenvalues of the new Jacobian (16) is evaluated as $\lambda_{1,2}(A) = \frac{-e^{10} \pm \sqrt{e^{20} - 4e^{10}}}{4}$ with $\tau = \Omega(10^5)$.

C A condition of choosing the regularization matrix

First, we note that the regularization matrix Γ introduced by a good Jacobian regularization method cannot be arbitrary and a particular condition is given as follows.

Condition 1 (Non-Reversing-Flow Condition). *By applying the regularization matrix Γ , it should not reverse the overall gradient flow for the original minimax problem (1).*

A counterexample of the Non-Reversing-Flow Condition is to choose $\Gamma = -M^T$ where $M \triangleq \frac{\partial \tilde{\nabla} f(w^{(k)})}{\partial w^{(k)}}$ such that the new Jacobian becomes $A = -M^T M$ which is a Hessian with no complex eigenvalues and thus it could avoid the *Phase Factor*. From (6), the updates become

$$\begin{aligned} w^{(k+1)} &= w^{(k)} - \eta M^T \tilde{\nabla} f(w^{(k)}) \\ &= w^{(k)} - \eta \nabla^2 f(w^{(k)}) \nabla f(w^{(k)}) \end{aligned}$$

As we know, in general, the objective $f(\phi, \theta)$ is not convex-concave in ϕ and θ . For example, $f(\phi, \theta)$ becomes concave-concave in ϕ and θ near the equilibrium in the simple vanilla GAN example (3). Therefore, for any $w^{(k)}$ satisfying $\nabla_{\phi\phi}^2 f(w^{(k)}) \prec 0$, particularly if assuming $\nabla_{\phi\phi}^2 f(w^{(k)}) = -t^2 I$ where t is a non-zero scalar, the update for ϕ becomes

$$\phi^{(k+1)} = \phi^{(k)} + \eta t^2 \nabla_{\phi} f(w^{(k)}) - \eta \nabla_{\theta\phi}^2 f(w^{(k)}) \nabla_{\theta} f(w^{(k)})$$

According to the first two terms on the right-hand side of the above equation, it is actually a gradient flow of the generator G_ϕ maximizing the objective $f(\phi, \theta)$ instead. This partly explains why directly minimizing a surrogate loss $l(w) = \frac{1}{2} \|\nabla f(w^{(k)})\|^2$ does not work well in practice as has been observed by [15].

Next, we point out that ConOpt may also violate the Non-Reversing-Flow Condition in some cases. Similarly, for any point $w^{(k)}$ satisfying $\nabla_{\phi\phi}^2 f(w^{(k)}) \prec 0$, particularly if we assume $\nabla_{\phi\phi}^2 f(w^{(k)}) = -t^2 I$, the update for ϕ in (9) for ConOpt becomes

$$\phi^{(k+1)} = \phi^{(k)} + \eta(\gamma t^2 - 1) \nabla_{\phi} f(w^{(k)}) - \eta \gamma \nabla_{\theta\phi}^2 f(w^{(k)}) \nabla_{\theta} f(w^{(k)})$$

If $\gamma t^2 > 1$, it is also a gradient flow of the generator G_ϕ maximizing the objective $f(\phi, \theta)$ instead. Note that the Hessian $\nabla_{\phi\phi}^2 f(w^{(k)})$, introduced by ConOpt to the parameter updates, serves as the root cause of violating Condition 1. This might also partly explains why ConOpt is less robust than our proposed method in some experiments. Even worse, as γ increases, it is more likely for ConOpt to reverse the gradient flow. It intuitively explains why γ should be kept relatively small for ConOpt.

D Proofs in Section 4

D.1 Proof of Theorem 2

Proof. we revisit each of these three regularization methods by evaluating and analyzing the eigenvalues of their Jacobians in the simple vanilla GAN example separately.

Only regularizing generator. In the simple vanilla GAN example, from (5) in Lemma 1 we have $\frac{\partial \tilde{\nabla} f(w^{(k)})}{\partial w^{(k)}} = \begin{bmatrix} 0 & \frac{1}{2}I \\ -\frac{1}{2}I & -\frac{1}{2}(\sigma^2 I + vv^T) \end{bmatrix}$. Also the regularization matrix becomes $\Gamma = \begin{bmatrix} I & \frac{\gamma}{2}I \\ 0 & I \end{bmatrix}$. Thus, for all points in $B_\delta(w^*)$, the Jacobian is

$$A = \Gamma \frac{\partial \tilde{\nabla} f(w^{(k)})}{\partial w^{(k)}} = \begin{bmatrix} I & \frac{\gamma}{2}I \\ 0 & I \end{bmatrix} \begin{bmatrix} 0 & \frac{1}{2}I \\ -\frac{1}{2}I & -\frac{1}{2}(\sigma^2 I + vv^T) \end{bmatrix} = \begin{bmatrix} -\frac{\gamma}{4}I & \frac{1}{2}I - \frac{\gamma}{4}(\sigma^2 I + vv^T) \\ -\frac{1}{2}I & -\frac{1}{2}(\sigma^2 I + vv^T) \end{bmatrix}$$

By definition of eigenvalues, let $Ay = \lambda y$ where $y = \begin{bmatrix} y_1 \\ y_2 \end{bmatrix} \neq 0$, then

$$-\frac{\gamma}{4}y_1 + \left(\frac{1}{2}I - \frac{\gamma}{4}(\sigma^2 I + vv^T) \right) y_2 = \lambda y_1 \quad (17)$$

$$-\frac{1}{2}y_1 - \frac{1}{2}(\sigma^2 I + vv^T) y_2 = \lambda y_2 \quad (18)$$

From (17) we have $y_1 = \frac{1}{\lambda + \frac{\gamma}{4}} \left(\frac{1}{2}I - \frac{\gamma}{4}(\sigma^2 I + vv^T) \right) y_2$ (note that $\lambda \neq -\frac{\gamma}{4}$; otherwise, we get $y = 0$). Plugging it into (18) yields

$$-\lambda vv^T y_2 = \left(2\lambda^2 + \left(\frac{1}{2}\gamma + \sigma^2 \right)\lambda + \frac{1}{2} \right) y_2 \quad (19)$$

Similarly, we can also solve (19) in two cases yielding the eigenvalues of the Jacobian as follows,

$$\lambda_{1,2}(A) = \frac{-(\sigma^2 + \frac{\gamma}{2}) \pm \sqrt{(\sigma^2 + \frac{\gamma}{2})^2 - 4}}{4}, \quad \lambda_{3,4}(A) = \frac{-(\beta^2 + \frac{\gamma}{2}) \pm \sqrt{(\beta^2 + \frac{\gamma}{2})^2 - 4}}{4} \quad (20)$$

As we can see, the resulting $\zeta = \sqrt{(\frac{2}{\sigma^2 + \frac{\gamma}{2}})^2 - 1}$ for $\sigma^2 + \frac{\gamma}{2} < 2$, which means increasing γ will decrease ζ and thus could alleviate the impact of the *Phase Factor* by Corollary 1. However, the resulting $\tau = \frac{((\beta^2 + \frac{\gamma}{2}) + \sqrt{(\beta^2 + \frac{\gamma}{2})^2 - 4})^2}{4}$ for $\beta^2 + \frac{\gamma}{2} > 2$, which means increasing γ will also increase τ and thus the impact of *Conditioning Factor* will not be alleviated but become much severer by Corollary 2. Therefore, if the *Conditioning Factor* is the main obstacle for the GAN convergence (for example, $\|v\|$ is sufficiently large in the simple vanilla GAN example), only regularizing generator as in (7) will make the convergence performance of the GAN training worse.

Smoothing optimizer. Similarly in the simple vanilla GAN example, the regularization matrix becomes $\Gamma = \begin{bmatrix} I & 0 \\ -\frac{\gamma}{2}I & I \end{bmatrix}$. For any point in $B_\delta(w^*)$, the Jacobian is

$$A = \Gamma \frac{\partial \tilde{\nabla} f(w^{(k)})}{\partial w^{(k)}} = \begin{bmatrix} I & 0 \\ -\frac{\gamma}{2}I & I \end{bmatrix} \begin{bmatrix} 0 & \frac{1}{2}I \\ -\frac{1}{2}I & -\frac{1}{2}(\sigma^2 I + vv^T) \end{bmatrix} = \begin{bmatrix} 0 & \frac{1}{2}I \\ -\frac{1}{2}I & -\frac{1}{2}((\sigma^2 + \frac{\gamma}{2})I + vv^T) \end{bmatrix}$$

Then by following from the exact proof of Theorem 1 after replacing σ^2 in the Jacobian of (11) by $\sigma^2 + \frac{\gamma}{2}$, we can get the eigenvalues of the Jacobian as follows,

$$\lambda_{1,2}(A) = \frac{-(\sigma^2 + \frac{\gamma}{2}) \pm \sqrt{(\sigma^2 + \frac{\gamma}{2})^2 - 4}}{4}, \quad \lambda_{3,4}(A) = \frac{-(\beta^2 + \frac{\gamma}{2}) \pm \sqrt{(\beta^2 + \frac{\gamma}{2})^2 - 4}}{4} \quad (21)$$

As the eigenvalues here are exactly the same with (20), the local convergence properties of only regularizing the discriminator are identical to those of only regularizing the generator. Similarly, if *Conditioning Factor* becomes the main obstacle for GAN convergence, only regularizing discriminator as in (8) will make the convergence performance of the GAN training worse.

Consensus optimization (ConOpt). Since for ConOpt, it is a little bit tricky to obtain the eigenvalues of its Jacobian directly, we turn to comparing the eigenvalues of its Jacobian with those of the Jacobian for SimGD.

First, we define $M \triangleq \frac{\partial \tilde{\nabla} f(w^{(k)})}{\partial w^{(k)}}$. For SimGD, we know its Jacobian is M . For ConOpt, since the regularization matrix $\Gamma = I - \gamma M^T$, its Jacobian is given by

$$A = \Gamma M = M - \gamma M^T M \quad (22)$$

Then, we define $\bar{\lambda}(M)$ and $\underline{\lambda}(M)$ as the two eigenvalues of M with the largest and smallest absolute values, respectively, and the similar definitions of $\bar{\lambda}(A)$ and $\underline{\lambda}(A)$ apply to A . As a result, the condition numbers of A and M are given by $\tau(A) \triangleq \frac{|\bar{\lambda}(A)|}{|\underline{\lambda}(A)|}$ and $\tau(M) \triangleq \frac{|\bar{\lambda}(M)|}{|\underline{\lambda}(M)|}$, respectively.

If $\sigma^2 < 2$ and $\beta^2 > 2$, from Theorem 1 we know for any point in $B_\delta(w^*)$, the Jacobian for SimGD satisfies $|\lambda_{1,2}(M)| = \frac{1}{2}$, $|\lambda_3(M)| = \frac{\beta^2 + \sqrt{(\beta^2)^2 - 4}}{4} > \frac{1}{2}$ and $|\lambda_4(M)| = \frac{\beta^2 - \sqrt{(\beta^2)^2 - 4}}{4} < \frac{1}{2}$. Thus, $\bar{\lambda}(M) = \lambda_3(M)$ and $\underline{\lambda}(M) = \lambda_4(M)$, which are both negative real values.

By definition of eigenvalues, we have $My_1 = \bar{\lambda}(M)y_1$ and $My_2 = \underline{\lambda}(M)y_2$ where y_1 and y_2 are two normalized eigenvectors of M with unit length. Thus, $y_1^T My_1 = \bar{\lambda}(M)$ and $y_2^T My_2 = \underline{\lambda}(M)$. From (22), we have $y_1^T My_1 = \bar{\lambda}(M) - \gamma \bar{\lambda}(M)^2$ and $y_2^T My_2 = \underline{\lambda}(M) - \gamma \underline{\lambda}(M)^2$. From the definition of $\bar{\lambda}(A)$ and $\underline{\lambda}(A)$, we know $|y_1^T Ay_1| \leq |\bar{\lambda}(A)|$ and $|y_2^T Ay_2| \geq |\underline{\lambda}(A)|$, then $|\bar{\lambda}(M) - \gamma \bar{\lambda}(M)^2| \leq |\bar{\lambda}(A)|$ and $|\underline{\lambda}(M) - \gamma \underline{\lambda}(M)^2| \geq |\underline{\lambda}(A)|$. Combining the two inequalities yields

$$\tau(A) \geq \tau(M) \cdot \frac{1 + \gamma |\bar{\lambda}(M)|}{1 + \gamma |\underline{\lambda}(M)|} \quad (23)$$

Define by $\Delta(\gamma) \triangleq \frac{1+\gamma|\bar{\lambda}(M)|}{1+\gamma|\lambda(M)|}$. As $|\bar{\lambda}(M)| > |\lambda(M)| > 0$ and $\gamma > 0$, we have $\Delta(\gamma) > 1$, which means $\tau(A) > \tau(M)$ for any $\gamma > 0$. Even worse, since the derivative $\Delta'(\gamma) = \frac{\bar{\lambda}(M)-\lambda(M)}{(1-\gamma\bar{\lambda}(M))^2} > 0$, when γ increases, $\Delta(\gamma)$ also increases. Thus, by using ConOpt, the impact of *Conditioning Factor* is not alleviated but becomes more severe by Corollary 2. Furthermore, the Jacobian will be worse-conditioned with the increment of γ . Therefore, although ConOpt could alleviate the impact of the *Phase Factor* as shown in [15], it will make the GAN convergence performance worse if the *Conditioning Factor* becomes the main obstacle for the GAN convergence.

From the above analysis, we can see that all these three gradient-based regularization methods cannot alleviate the *Phase Factor* and *Conditioning Factor* simultaneously. \square

D.2 Proof of Theorem 3

Proof. When applying the proposed Jacobian regularization in the simple vanilla GAN example (3), the regularization matrix becomes $\Gamma = \begin{bmatrix} I & \frac{\gamma}{2}I \\ -\frac{\gamma}{2}I & I \end{bmatrix}$. Therefore, for any point in $B_\delta(w^*)$,

$$A = \Gamma \frac{\partial \tilde{\nabla} f(w^{(k)})}{\partial w^{(k)}} = \begin{bmatrix} I & \frac{\gamma}{2}I \\ -\frac{\gamma}{2}I & I \end{bmatrix} \begin{bmatrix} 0 & \frac{1}{2}I \\ -\frac{1}{2}I & \frac{1}{2}(\sigma^2 I + vv^T) \end{bmatrix} = \begin{bmatrix} -\frac{\gamma}{4}I & \frac{1}{2}I - \frac{\gamma}{4}(\sigma^2 I + vv^T) \\ -\frac{1}{2}I & -\frac{\gamma}{4}I - \frac{1}{2}(\sigma^2 I + vv^T) \end{bmatrix}$$

By definition of eigenvalues, let $Ay = \lambda y$ where $y = \begin{bmatrix} y_1 \\ y_2 \end{bmatrix} \neq 0$, then

$$-\frac{\gamma}{4}y_1 + \left(\frac{1}{2}I - \frac{\gamma}{4}(\sigma^2 I + vv^T)\right)y_2 = \lambda y_1 \quad (24)$$

$$-\frac{1}{2}y_1 - \frac{\gamma}{4}y_2 - \frac{1}{2}(\sigma^2 I + vv^T)y_2 = \lambda y_2 \quad (25)$$

Similarly, $\lambda \neq 0$, otherwise, we get $y = 0$ which violates the definition of eigenvectors. By applying (24) – (25) * $\frac{\gamma}{2}$, we have $y_1 = \frac{1}{\lambda} \left(\frac{\gamma}{2}\lambda + \frac{\gamma^2}{8} + \frac{1}{2} \right) y_2$. Plugging it into (25) yields

$$-\lambda vv^T y_2 = \left(2\lambda^2 + (\gamma + \sigma^2)\lambda + \frac{\gamma^2}{8} + \frac{1}{2} \right) y_2 \quad (26)$$

Similarly, we can solve (26) in two cases yielding the desired results by following the same process in the proof of Theorem 1. \square

D.3 Proof of Corollary 3

Proof. From Theorem 3 we know for $\sigma^2 < 2$, $\lambda_{1,2}(A)$ are complex eigenvalues only if $\gamma < \frac{2}{\sigma^2} - \frac{\sigma^2}{2}$. According to the above definition of ζ , we get

$$\zeta = \begin{cases} \sqrt{h_1(\gamma) - 1}, & \gamma < \frac{2}{\sigma^2} - \frac{\sigma^2}{2} \\ 0, & \gamma \geq \frac{2}{\sigma^2} - \frac{\sigma^2}{2} \end{cases} \quad (27)$$

where $h_1(\gamma) = \frac{\gamma^2 + 4}{(\sigma^2 + \gamma)^2} > 1$. Since the derivative of $h_1(\gamma)$ satisfies $h'_1(\gamma) = \frac{2(\gamma + \sigma^2)(\sigma^2\gamma - 4)}{(\sigma^2 + \gamma)^4} < 0$ and ζ is a monotonically increasing function of $h_1(\gamma)$ for $\gamma < \frac{2}{\sigma^2} - \frac{\sigma^2}{2}$, ζ is a monotonically decreasing function of γ for $\gamma < \frac{2}{\sigma^2} - \frac{\sigma^2}{2}$. As $\zeta = 0$ if $\gamma \geq \frac{2}{\sigma^2} - \frac{\sigma^2}{2}$, by the continuity of the function in (27), we have ζ is a monotonically decreasing function of γ where $\zeta \rightarrow 0$ as $\gamma \rightarrow \infty$. It means that we can increase γ to alleviate the impact of the *Phase Factor*.

Furthermore, from Theorem 3 we know for $\beta^2 > 2$,

$$\tau = \left(\sqrt{h_2(\gamma)} + \sqrt{h_2(\gamma)^2 - 1} \right)^2 \quad (28)$$

where $h_2(\gamma) = \frac{(\beta^2 + \gamma)^2}{\gamma^2 + 4} > 1$. Since the derivative of $h_2(\gamma)$ satisfies $h'_2(\gamma) = \frac{2(\gamma + \beta^2)(4 - \beta^2\gamma)}{(\gamma + 4)^4} < 0$ for $\gamma > \frac{4}{\beta^2}$ and τ is a monotonically increasing function of $h_2(\gamma)$, τ is a monotonically decreasing

function of γ for $\gamma > \frac{4}{\beta^2}$. As $\beta^2 > 2$, then $\frac{4}{\beta^2} < 2$ and we thus can safely replace the above condition $\gamma > \frac{4}{\beta^2}$ by $\gamma \geq 2$. In the limit of $\gamma \rightarrow \infty$, we have $h_2(\gamma) \rightarrow 1$ and thus from (28) $\tau \rightarrow 1$. It means that we can increase γ to alleviate the impact of the *Conditioning Factor* for all $\gamma > \frac{4}{\beta^2}$.

Therefore, it is reasonable to keep increasing the tunable parameter γ so as to alleviate or even eliminate both the *Phase Factor* and *Conditioning Factor* simultaneously, which demonstrates the advantages of JR-GAN. \square

E More experimental results

E.1 More results on Isotropic Gaussian

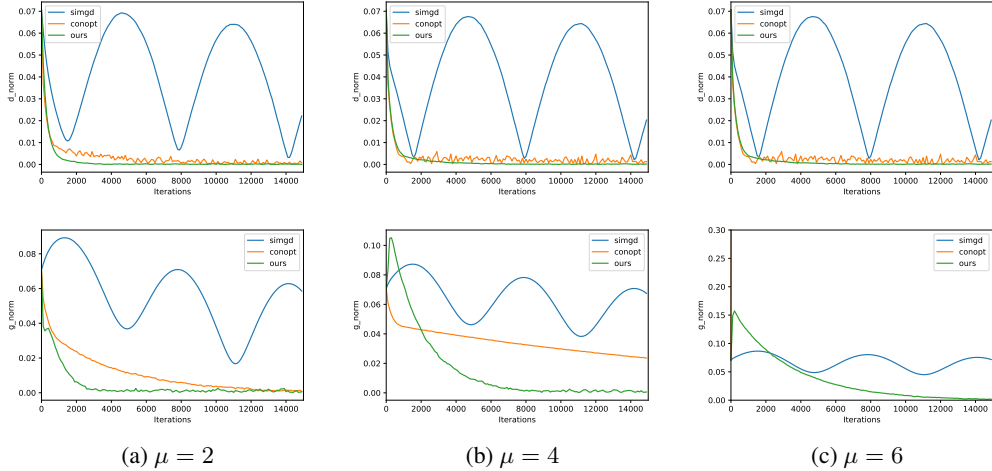


Figure 5: Training dynamics of SimGD, ConOpt and Ours with varying mean value μ where $\sigma = 0.2$. The top row shows the discriminator convergence and the bottom row shows the generator convergence. Note that as μ increases, the convergence rate for either SimGD or ConOpt becomes slower. When $\mu = 6$, the generator training curve for the ConOpt directly blow up.

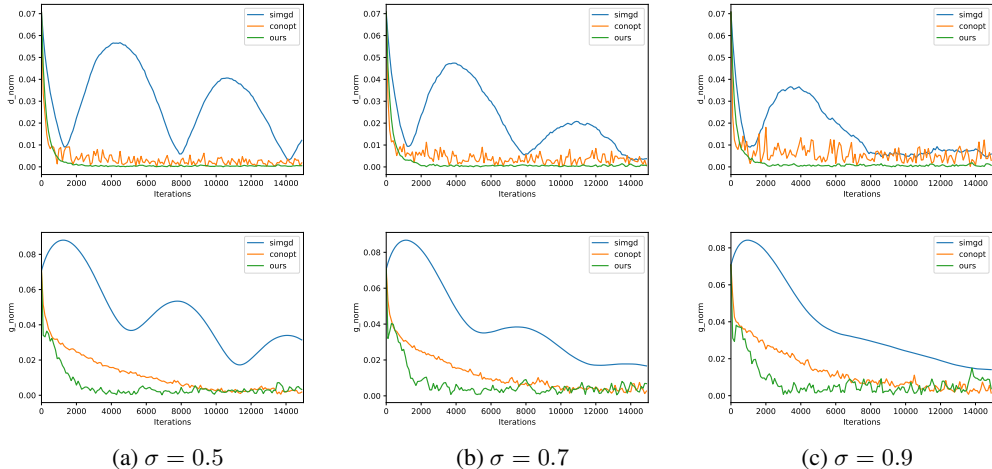


Figure 6: Training dynamics of SimGD, ConOpt and Ours with varying standard deviation σ where $\mu = 2$. The top row shows the discriminator convergence and the bottom row shows the generator convergence. Note that the damping effect in SimGD becomes stronger as the standard derivation σ increases.

Mixture of Gaussians. We systematically conduct more experiments on comparing SimGD, ConOpt and JR-GAN (Ours) on the data generated by a circular mixture of Gaussians, and the results are shown in Figure 7 and 8.

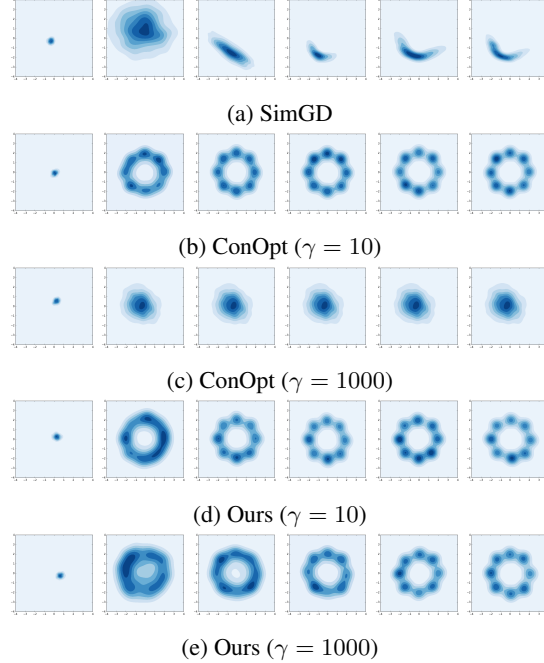


Figure 7: Comparison of SimGD (a), ConOpt (b,c) and Ours (d,e) on the mixture of Gaussians over iterations where $r = 2$. From left to right, each row consists of the results after 0, 2000, 4000, 6000, 8000 and 10000 iterations. Note that we present two results of both ConOpt and Ours by setting $\gamma \in \{10, 1000\}$, respectively.

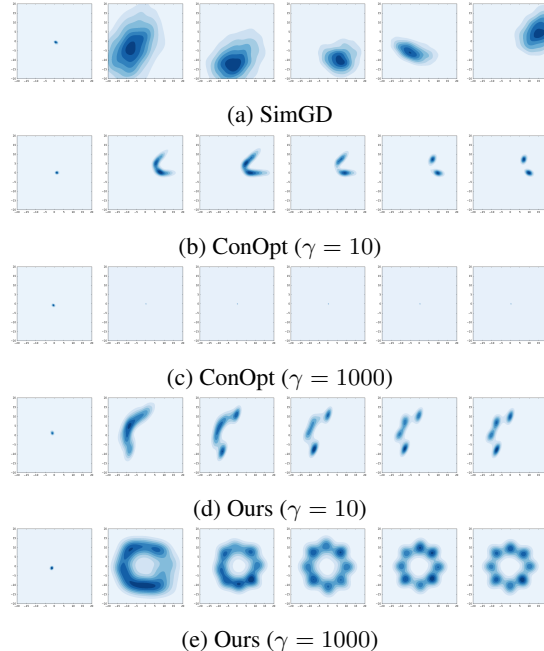


Figure 8: Comparison of SimGD (a), ConOpt (b,c) and Ours (d,e) on the mixture of Gaussians over iterations where $r = 10$. From left to right, each row consists of the results after 0, 2000, 4000, 6000, 8000 and 10000 iterations. Note that we present two results of both ConOpt and Ours by setting $\gamma \in \{10, 1000\}$, respectively.

E.2 Network architectures

| |
|---|
| $z \in \mathbb{R}^{128} \sim \mathcal{N}(0, I)$ |
| dense, $2 \times 2 \times M_f$ |
| 4×4 , stride=2, deconv. M_f ReLU |
| ResBlock M_f |
| 4×4 , stride=2, deconv. M_f ReLU |
| ResBlock M_f |
| 4×4 , stride=2, deconv. M_f ReLU |
| ResBlock M_f |
| 4×4 , stride=2, deconv. 3 tanh |

(a) Generator

| |
|--|
| $x \in \mathbb{R}^{32 \times 32 \times 3}$ |
| 4×4 , stride=2, conv. M_f ReLU |
| ResBlock M_f |
| 4×4 , stride=2, conv. M_f ReLU |
| ResBlock M_f |
| 4×4 , stride=2, conv. M_f ReLU |
| ResBlock M_f |
| 4×4 , stride=2, conv. M_f ReLU |
| ResBlock M_f |
| 4×4 , stride=2, conv. M_f ReLU |
| ResBlock M_f |
| dense $\rightarrow 1$ |

(b) Discriminator

Table 2: ResNet architectures v1 for CIFAR-10 where M_f denotes the number of filters.

| |
|---|
| $z \in \mathbb{R}^{128} \sim \mathcal{N}(0, I)$ |
| dense, $4 \times 4 \times M_f$ |
| 4×4 , stride=2, deconv. M_f ReLU |
| ResBlock M_f |
| 4×4 , stride=2, deconv. M_f ReLU |
| ResBlock M_f |
| 4×4 , stride=2, deconv. M_f ReLU |
| ResBlock M_f |
| 3×3 , stride=1, conv. 3 tanh |

(a) Generator

| |
|--|
| $x \in \mathbb{R}^{32 \times 32 \times 3}$ |
| 4×4 , stride=2, conv. M_f ReLU |
| ResBlock M_f |
| 4×4 , stride=2, conv. M_f ReLU |
| ResBlock M_f |
| 4×4 , stride=2, conv. M_f ReLU |
| ResBlock M_f |
| 4×4 , stride=2, conv. M_f ReLU |
| ResBlock M_f |
| 4×4 , stride=2, conv. M_f ReLU |
| ResBlock M_f |
| dense $\rightarrow 1$ |

(b) Discriminator

Table 3: ResNet architectures v2 for CIFAR-10 where M_f denotes the number of filters.

| |
|---|
| $z \in \mathbb{R}^{128} \sim \mathcal{N}(0, I)$ |
| dense, $4 \times 4 \times M_f$ |
| 4×4 , stride=2, deconv. M_f ReLU |
| ResBlock M_f |
| 4×4 , stride=2, deconv. M_f ReLU |
| ResBlock M_f |
| 4×4 , stride=2, deconv. M_f ReLU |
| ResBlock M_f |
| 4×4 , stride=2, deconv. M_f ReLU |
| ResBlock M_f |
| 3×3 , stride=1, conv. 3 tanh |

(a) Generator

| |
|--|
| $x \in \mathbb{R}^{64 \times 64 \times 3}$ |
| 4×4 , stride=2, conv. M_f ReLU |
| ResBlock M_f |
| 4×4 , stride=2, conv. M_f ReLU |
| ResBlock M_f |
| 4×4 , stride=2, conv. M_f ReLU |
| ResBlock M_f |
| 4×4 , stride=2, conv. M_f ReLU |
| ResBlock M_f |
| 4×4 , stride=2, conv. M_f ReLU |
| ResBlock M_f |
| 4×4 , stride=2, conv. M_f ReLU |
| ResBlock M_f |
| dense $\rightarrow 1$ |

(b) Discriminator

Table 4: ResNet architectures for CelebA where M_f denotes the number of filters.

| |
|---|
| $z \in \mathbb{R}^{128} \sim \mathcal{N}(0, I)$ |
| dense, $4 \times 4 \times M_f$ |
| 4×4 , stride=2, deconv. M_f ReLU |
| ResBlock M_f |
| 4×4 , stride=2, deconv. M_f ReLU |
| ResBlock M_f |
| 4×4 , stride=2, deconv. M_f ReLU |
| ResBlock M_f |
| 4×4 , stride=2, deconv. M_f ReLU |
| ResBlock M_f |
| 4×4 , stride=2, deconv. M_f ReLU |
| ResBlock M_f |
| 3×3 , stride=1, conv. 3 tanh |

(a) Generator

| |
|--|
| $x \in \mathbb{R}^{128 \times 128 \times 3}$ |
| 4×4 , stride=2, conv. M_f ReLU |
| ResBlock M_f |
| 4×4 , stride=2, conv. M_f ReLU |
| ResBlock M_f |
| 4×4 , stride=2, conv. M_f ReLU |
| ResBlock M_f |
| 4×4 , stride=2, conv. M_f ReLU |
| ResBlock M_f |
| 4×4 , stride=2, conv. M_f ReLU |
| ResBlock M_f |
| 4×4 , stride=2, conv. M_f ReLU |
| ResBlock M_f |
| 4×4 , stride=2, conv. M_f ReLU |
| ResBlock M_f |
| 3×3 , stride=1, conv. 3 tanh |

(b) Discriminator

Table 5: ResNet architectures for ImageNet where M_f denotes the number of filters.

E.3 Training time on CIFAR-10 with four methods: GAN, SN-GAN, ConOpt and Ours.

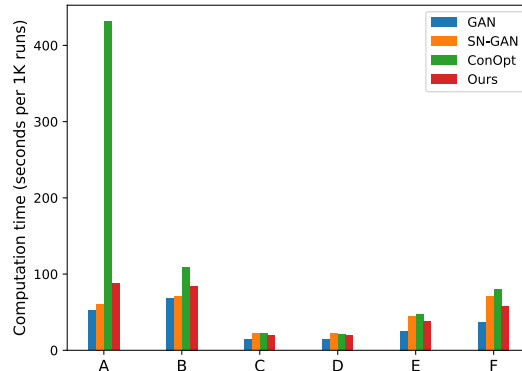


Figure 9: Training time on CIFAR-10 with four training methods: GAN, SN-GAN, ConOpt and Ours in all the A-F settings.

E.4 Generated images on CIFAR-10 with four methods: GAN, SN-GAN, ConOpt and Ours.

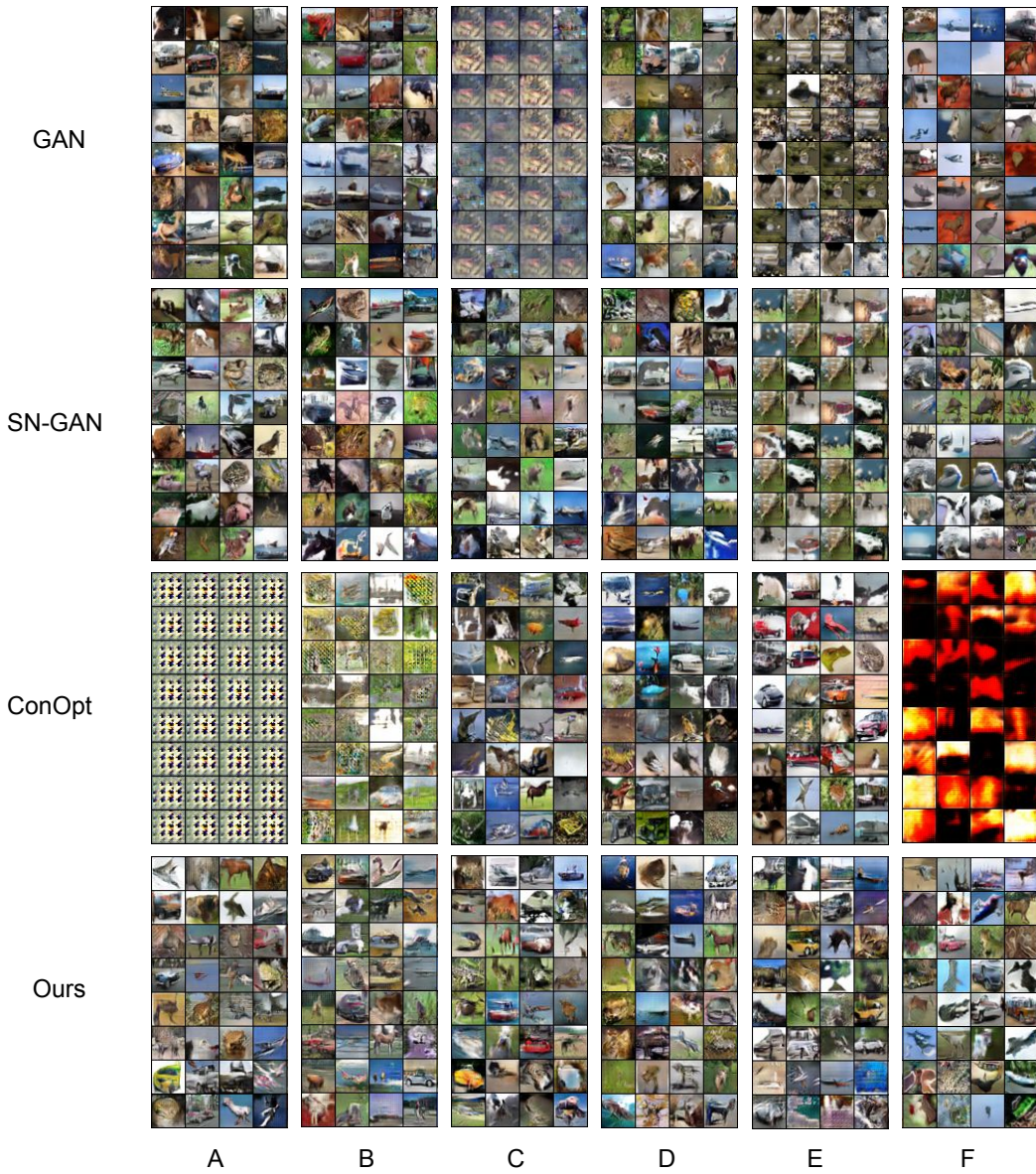


Figure 10: Generated images on CIFAR-10 with four training methods: GAN, SN-GAN, ConOpt and Ours in all the A-F settings. Best viewed in the electronic version by zooming in.